Article number 4596 Revision 1

Crystal structure and compressibility of lead dioxide up to 140 GPa

7/31/2013

B. Grocholski[1*] , S.-H. Shim[2], E. Cottrell[1] and V. B. Prakapenka[3]

[1]Department of Mineral Sciences, National Museum of Natural History, Smithsonian Institution, 10th & Constitution Ave., Washington DC, USA.

[2]School of Earth and Space Exploration, Arizona State University, Tempe, Arizona, USA.

[3] University of Chicago, Chicago, Illinois, USA.

[*] corresponding author (b.grocholski@gmail.com)

Abstract

Lead dioxide is an important silica analog that has high-pressure behavior similar to what has been predicted for silica, only at lower pressures. We have measured the structural evolution and compressional behavior of different lead dioxide polymorphs up to 140 GPa in the laser heated diamond-anvil cell using argon as a pressure medium. High temperature heating prevents the formation of multi-phase mixtures found in a previous study conducted at room temperature using a silicone grease pressure medium. We find diffraction peaks consistent with a baddeleyite-type phase in our cold-compressed samples between 30 and 40 GPa, which was not observed in the previous measurements. Lead dioxide undergoes a phase transition to a cotunnite-type phase at 24 GPa. This phase remains stable to at least 140 GPa with a bulk modulus of 219(3) GPa for K'_0=4. Decompression measurements show a pure cotunnite-type phase until 10.5 GPa, where the sample converts to a mixture of baddeleyite-type, pyrite-type, and OI-type (Pbca) phases. Pure α-structured lead dioxide (scrutinyite) is found after pressure release at room pressure even though

our starting material was in the β-structure (plattnerite). Pressure quenching to the α-structure appears to be a common feature of all group IVa oxides that are compressed to structures with greater density than the rutile-type structure.

1. Introduction

Lead dioxide, a silica analog compound, has a typical sequence of phase transitions for an AX_2-type compound (Prakapenka et al., 2003). Two forms are found as minerals on the Earth's surface, the orthorhombic α-PbO_2 structure (scrutinyite) and the tetragonal rutile structured β-PbO_2 phase (plattnerite). Previous results relying on cold-compression using a silicone grease pressure-transmitting medium showed that both structures converted to the pyrite-type structure (*Pa-3*) at 7 GPa, with plattnerite going through the $CaCl_2$-type (distorted-stishovite) phase at 4 GPa before adopting the cubic structure. The SrI_2-type or OI orthorhombic structure (*Pbca*) was found between 11 GPa to 47 GPa, with the cotunnite-type structure (*Pnam*) coexisting with it from 29 to at least 47 GPa at 300 K (Haines et al., 1996) (Fig. 1).

The cotunnite structure consists of highly-coordinated cations (nine-fold coordination) and a distorted hexagonal close packed (hcp) sub-lattice of anions common to metal dioxides, fluorides, and chlorides. The structure is remarkable not only due to its ubiquitous nature in AX_2 type compounds (Dewhurst and Lowther, 2001), but also because of the large volume change across the high-pressure transition from the pyrite-type or OI-type structures that are closely related in energy. Materials with the cotunnite structure are relatively incompressible with certain compounds (such as SnO_2 and TiO_2) having measured bulk moduli approaching diamond (Ahuja and Dubrovinsky, 2002; Shieh et al., 2006) and are intriguing possibilities for super-hard materials. The stability of highly coordinated structures for silica analogs have also been

recognized as being important for understanding the experimentally inaccessible interiors of large terrestrial extrasolar planets (Umemoto et al., 2006; Grocholski et al., 2010).

We have conducted experiments on the structural evolution of PbO_2 up to 140 GPa with the laser-heated diamond-anvil cell (LHDAC) using synchrotron X-ray diffraction (XRD). High quality diffraction patterns resulting from laser annealing in an argon surrounded sample allows for better determination of phase stability and compressibility of the high pressure phases of lead dioxide.

2. Experimental methods

We used β-PbO_2 (plattnerite, Alfa-Aesar, 99.995%) for the starting material. The crystal structure was confirmed using a Rigaku D/Max Rapid micro-X-ray diffractometer at the National Museum of Natural History. A total of four samples of pure β-PbO_2 were compressed into platelets and loaded into symmetric-type diamond-anvil cells with 300, 200, and 150 μm culets in sample chambers of 150, 120, and 90 μm, respectively. Pre-indented rhenium gaskets were used for all experiments. All samples were propped up on spacer grains of lead dioxide to allow cryogenically liquified argon to create a layer between the sample and the diamond culet. Argon acts as both a pressure medium and a thermal insulator. We used an X-ray transparent cBN seat to allow detection of diffraction peaks up to $2\theta \approx 21°$.

Pressure was determined up to 75 GPa with the use of ruby fluorescence (Mao et al., 1986) from chips placed along the edge of the sample chamber, up to 120 GPa with the use of the diamond Raman scale (Akahama and Kawamura, 2006), and from 120–140 GPa with the equation of state for argon (Ross et al., 1986). The pressure determined from the diamond scale and the argon equation of state agree within experimental uncertainty at 120 GPa. We assume no systematic offset in pressure between different calibrants, which could slightly change our bulk

modulus and extrapolated V_0. Measured pressures agreed within experimental error before and after the heating cycle. We do not include thermal pressures (Heinz, 1990) in the pressures reported for our high-temperature data, which should therefore be regarded as a lower bound.

X-ray diffraction patterns in the LHDAC were measured at sector 13 of the Advanced Photon Source (wavelength of 0.3344 Å). Due to the relatively large sample compared to the laser (~20 μm in diameter) and X-ray (3×4 μm^2) spot size (Prakapenka et al., 2008), several fresh (previously unheated) sample areas were heated at different pressures. Although the diffraction patterns of our cold-compressed samples look similar to the patterns measured under a silicone grease medium (Haines et al., 1996), the peak widths in our argon loaded samples are much smaller than the silicone grease results (Fig. 2). X-ray diffraction patterns were collected during each laser heating cycle to track the growth of the cotunnite-type phase. Lead dioxide absorbs the 1064 nm infrared laser beam (YDFL) very well, with cotunnite-type PbO_2 appearing immediately upon laser coupling (T<1300 K) above 24 GPa. The combination of annealing differential stress in the sample chamber and sample recrystallization results in very sharp diffraction peaks (Figs. 2, 3d, and 4b) in comparison to the unheated diffraction patterns (Figs. 3c and 4a).

We collected XRD patterns up to a pressure of 140 GPa. One sample was decompressed from 75 GPa after cotunnite synthesis to room pressure at room temperature in roughly 10 GPa steps. Unit cell refinements for all phases from the diffraction patterns were analyzed with the GSAS structural refinement package using Le Bail equally weighted refinements (Larson and Von Dreele, 2000). When we obtain smooth and sharp diffraction patterns of PbO_2 as a pure cotunnite-type phase we performed Reitveld refinement (Fig. 4b,c). We correct the absorption effect from the cBN seat, but exclude the region between 14.5° and 15.25° 2θ where the scattered

X-rays are going through the tapered part of the seat. We found intensity in this region to be extremely sensitive to the exact centering of the sample relative to the opening. The region happens to be where there are only a few expected diffraction peaks from the cotunnite structure and exclusion of the region does not greatly affect the precision of the refinement (~90 peaks for 17 variables). A Le Bail equally weighted refinement was used to first determine lattice, peak shape, and background fit parameters for all phases. These parameters were then fixed and a best fit was obtained by varying the atomic position and thermal parameters in Rietveld refinements for the cotunnite-type phase.

3. Results and Discussion

Plattnerite (β-PbO_2) is the more common of the two lead dioxide polymorphs and our starting material is in this structure. X-ray diffraction of the starting material confirmed the rutile structure. Initial room temperature compression of our PbO_2 samples resulted in the OI structure (Fig. 3a) at 14–39 GPa and the cotunnite-type (Fig. 3c) at 61–140 GPa. We find a few reflections between 29 and 39 GPa that cannot be fit with the OI structure and are likely due to baddeleyite-type PbO_2 (Fig. 3b). The most intense reflection of the baddeleyite-type can account for the peak at ~6.9° (*d*-spacing = 2.778 Å) in these diffraction patterns if we assume the volume is similar to the OI structure. The previous measurements from Haines et al. (1996) found formation of a mixture of OI and cotunnite-type phases instead in the 29–47 GPa pressure range. The most notable difference between Haines et al. (1996) and our measurements is that we used Ar whereas they used silicone grease for a pressure medium. The peak width in our cold-compression measurements are a factor of 2–3 narrower than in Haines et al. (1996) (Fig. 2), consistent with much higher deviatoric stresses from the silicone grease (Angel et al., 2007).

Therefore, the lower pressure appearance of the cotunnite-type phase in Haines et al. (1996) is probably related to larger deviatoric stresses from the silicon grease medium. The failure to observe the baddeleyite-type peaks in the previous result may have been due to peak broadening of the OI and cotunnite-type phases, obscuring diffraction peaks from the monoclinic phase if present in their samples.

The cotunnite-type phase of PbO_2 is stable after heating at 24 GPa and persists at high temperatures up to at least 140 GPa in our experiments (Figs 1 and 3c,d). As expected, the transition pressure is lower than analogs such as TiO_2 or SnO_2 that convert to the cotunnite-type from the OI structure at ~60 GPa (Dekura et al., 2011; Shieh et al., 2006). The wide stability field is also not surprising, as TiO_2 has experimentally been found to be stable from 60 to 200 GPa (Dekura et al., 2011) and compounds such as SiO_2 are extremely stable computationally in the cotunnite structure (Umemoto et al., 2006; Tsuchiya and Tsuchiya, 2011). Post-cotunnite phase transitions in oxide systems have been reported only rarely, but for TiO_2 the transition to a Fe_2P phase occurrs at ~200 GPa (Dekura et al., 2011). Several other structures have been suggested as well, including Ni_2In and Co_2Si, among others (Leger et al., 1995; Haines et al., 1998; Griffiths et al., 2009; Dorfman et al., 2010). Since PbO_2 appears to be a good analog for SiO_2 and Pb has a larger scattering cross section, it is a good candidate for exploring post-cotunnite structures for group IVa oxides. If the systematics of oxides follow similar behavior to the fluorides, where the pressure of the post-cotunnite transition decreases with increasing 1 bar cation radius (Dorfman et al., 2010), the post-cotunnite phase should become stable between the 140 GPa found in this experiment and 200 GPa as has been found for TiO_2.

The cotunnite-type is converted to a mixture of the OI, baddeleyite-type, and pyrite-type phases on cold decompression from 24 GPa to 10.5 GPa (Fig. 3e). The appearance of a small amount of baddeleyite structured PbO_2 is not surprising as the structure is commonly found in

other AX_2 compounds and is closely related in crystal structure to both OI and pyrite types (Dubrovinskaia et al., 2001; Lowther et al., 1999). The OI phase is likely metastable above 24 GPa, as low-temperature heating (T < 1300 K) immediately converts the OI structure to the cotunnite-type (Fig. 3a,b) and the cotunnite structure is stable on decompression to 24 GPa as well (Fig. 1). Pressure quenching from the OI, baddeleyite-type, and pyrite-type mixture produces scrutinyite (α-PbO_2, Fig. 3f), with no evidence of any material reverting to the rutile structure (β-PbO_2).

Retention of the α-PbO_2 structure is common among all the group IVa oxides. Once the structure is formed it can be quenched to room pressure as in the case of SiO_2 (Dubrovinsky et al., 1997; Grocholski et al., 2013) and GeO_2 (Prakapenka et al., 2003). Transformation to even higher coordination structures such as the pyrite-type in the case of SnO_2 (Haines and Leger, 1997) or the cotunnite-type for PbO_2 (Haines et al., 1996) still retain the scrutinyite (α-PbO_2) structure over conversion to the more stable rutile (β-PbO_2) structure on decompression. The reason for this is likely due to the unfavorable transformation path through the baddeleyite structure required to convert back to the rutile structure (Haines and Leger, 1997). Intriguingly, PbO_2, TiO_2, and SiO_2 have been synthesized in the α-PbO_2 structure through purely metastable pathways (Carr and Hampson, 1972; Chen and Shen, 2002; Dubrovinsky et al., 2001a), as well as been found in nature (Taggart et al., 1988; El Goresy et al., 2001kb; Sharp et al., 1999). This observation suggests that for the remaining group IVa oxides (SnO_2 and GeO_2) we should expect to find specimens with the scrutinyite structure in nature either from the shock processes that have been shown to form α-PbO_2-type TiO_2 (El Goresy et al., 2001kb) and SiO_2 (Sharp et al., 1999), or more speculatively as an oxidation product from hydrothermal mineralization as is the case for PbO_2 (Taggart et al., 1988).

The sequence of phase transitions is consistent with the previous experiments on PbO_2 (Haines et al., 1996) and SnO_2 (Haines and Leger, 1997; Shieh et al., 2006). The phases of PbO_2 are also close to the alkali earth fluorides, although some adopt the cubic fluoride structure and the OI structure is not stable (Dorfman et al., 2010; Grocholski et al., 2010). The phase sequence is similar to experimental results on the group IV oxides, except these compounds transform to the monoclinic baddeleyite-type phase before transforming to the OI structure (Ohtaka et al., 2001a, b). Our experiments cannot rule out a small stability field for the baddeleyite-type structure between 10 and 11 GPa (Fig. 3e), and the structure may stabilize with temperature. The baddeleyite-type structure is likely metastable along with the OI structure above 30 GPa (Fig. 3a), as heating this assemblage above 30 GPa results in the cotunnite structure (Fig. 1).

A typical diffraction pattern of the cotunnite-type structure is shown in Fig. 4c with the atomic structure obtained from Rietveld refinement shown in Fig. 5. The refined crystal structure has atomic coordinates similar to other cotunnite-type phases including the previous refinement on PbO_2. However, the previous refinement on PbO_2 was conducted on a cold-compressed sample that was a mixture of cotunnite-type and OI-type structures (Haines et al., 1996). The improvement on diffraction peak sharpness is two orders of magnitude from the older study (Fig. 2), due to high temperature heating of the sample that allows for the full conversion of the OI phase to the cotunnite phase and relieving differential stresses (Fig. 4) in the sample chamber (Heinz and Jeanloz, 1987; Fiquet et al., 1996). Our results also extend the *d*-space range from ~1.3 Å to ~0.9 Å, doubling the number of diffraction peaks included in each refinement from 45 to 93.

Our data set allows for the determination of six independent Pb–O bond lengths for the nine nearest neighbor oxygens and two co-planar Pb-Pb-Pb angles (Fig. 6). The bond lengths

(normalized to unit cell volume) and angles are consistent with other cotunnite structured compounds including $CaCl_2$, $BaCl_2$, TiO_2, and SnO_2 (Leger et al., 1998; Dubrovinsky et al., 2001b; Shieh et al., 2006). The normalized bond lengths for our PbO_2 data are closest to ZrO_2 (Desgreniers and Lagarec, 1999), which has a similar ionic radius. In general the Pb–O bond lengths decrease with increasing pressure, with the exception of the smallest Pb–O bond at 24 GPa (#4 in Fig. 5). The trend is for the bond lengths to become more regular as pressure increases, although the convergence levels off above 80 GPa. In general, the oxygen network stays as a distorted hcp lattice up to 140 GPa with no evidence of a displacive transition to a regular hcp lattice expected from most of the predicted post-cotunnite structures. Co-planar Pb-Pb-Pb angles similarly do not move towards 60°, but rather become slightly less regular as a function of pressure (Fig. 6c). Atomic coordinates for each structural refinement are given in Tab. 1.

Lattice parameters (Figs 7, 8, and Tab. 2) are generally in agreement with previous results (Haines et al., 1996). Lattice parameters for the pyrite-type and α structures agree within 1%, while the cotunnite lattice parameters are in agreement within experimental error up to 47 GPa. Compression is almost isotropic for the cotunnite-type phase, with the *b* axis slightly more and the *c* axis slightly less compressible than the *a* axis (Tab. 3). Our measured lattice parameters for the OI phase are smaller by up to 2% for *a* and *c* compared to the previous results. The *a* and *c* directions are also the most compressible, as the axial incompressibility in the *b* direction is more than three times greater (Tab. 3). The larger lattice parameters from Haines et al., (1996) are due to either greater deviatoric stresses from the use of silicone grease pressure medium or peak interferences from the cotunnite-type phase that appears in their samples.

Our axial ratios for both the OI and the cotunnite structures are in the range of those found for similar compounds (Dewhurst and Lowther, 2001). Our results show the *a*/*c* ratio for the

cotunnite-type structure increasing to 40 GPa, where it flattens and slightly decreases above 120 GPa. A flat *a*/*c* ratio is seen also in SnO_2 (Shieh et al., 2005) and ZrO_2 (Ohtaka et al., 2005), although the ratio is higher in these compounds. The decrease at 120 GPa may be indicative of a phase transformation coming at slightly higher pressure, as in the case for the alkali fluorides such as CaF_2 (Dorfman et al., 2010) that have sharply decreasing *a*/*c* ratio with pressure as the post-cotunnite transition is approached (Fig. 7).

The volume collapse between the OI and cotunnite structures is about 11% (Fig. 9), consistent with previous results on PbO_2 and other cotunnite-type phases (Haines et al., 1996; Dewhurst and Lowther, 2001). The change in volume with pressure was fit with a second-order Birch-Murnaghan equation for both the OI and cotunnite-type phases. Both fits were computed to minimize the error on K_0 and V_0 simultaneously. We included data up to 29 GPa from Haines et al. (1996) for the OI structure, but exclude parameters reported at higher pressures where large overlap in peak intensity occurs in the older experiments with the cotunnite-type phase. Our results indicate that the OI structure is more compressible (K_0 = 122(7) GPa) than previously measured by 2.5% using V_0 of 313.8(1.9) Å^3. The compressibility and room pressure volume of the cotunnite phase is remarkably consistent with the previous data, having a K_0 = 219(3) GPa and V_0 = 134.4(3) Å^3.

Our data significantly reduces the error on the bulk modulus and theoretical room pressure volume of the cotunnite-type phase of PbO_2. Unlike other silica analog compounds, the bulk modulus of the cotunnite-type phase is not significantly higher than the bulk modulus of other PbO_2 phases. The trend of increasing bulk moduli with decreasing ionic radii still holds, as compounds such as SnO_2 (Shieh et al., 2006) and possibly TiO_2 (Ahuja and Dubrovinsky, 2002; Al-Khatatbeh et al., 2009) being much less compressible than PbO_2. Cotunnite structured GeO_2

and SiO_2 should be very stiff as well and potential candidates for superhard materials, as predicted by computational studies (Teter, 1998; Dewhurst and Lowther, 2001).

We have conducted experiments on PbO_2 up to 140 GPa surrounded by an argon pressure medium in the LHDAC. Laser heating helps to prevent metastable phases from being present in the sample chamber that can occur under cold compression and to anneal differential stresses in the samples at high pressure. We find the cotunnite-type phase is stable from 24 GPa up to the highest pressure of this study (~140 GPa) at 300–3000 K (Fig. 1). We do not find a mixture of the OI and cotunnite-type phases under cold compression as was found in the previous results (Haines et al., 1996), but we do confirm the OI phase and baddeleyite-structured phase to be metastable under lower differential stress conditions up to 39 GPa. We also identify a mixed phase of baddeleyite, OI, and pyrite types at 10.5 GPa on decompression before full conversion to the α structure at 1 bar.

Acknowledgements

We would like to thank the two reviewers that provided helpful comments that improved this manuscript. We would also like to acknowledge technical assistance provided by Jeffrey Post at the National Museum of Natural History. This work was performed at GeoSoilEnviroCARS (Sector 13), Advanced Photon Source (APS), Argonne National Laboratory. GeoSoilEnviroCARS is supported by the National Science Foundation - Earth Sciences (EAR-1301813) and Department of Energy - Geosciences (DE-FG02-94ER14466). Use of the Advanced Photon Source was supported by the U. S. Department of Energy, Office of Science, Office of Basic Energy Sciences, under Contract No. DE-AC02-06CH11357. This work is supported by NSF to S.H.S. (EAR1301813) and by the Peter Buck Research Fellowship to B. G.

References

Ahuja, R., and Dubrovinsky, L. (2002) High-pressure structural phase transitions in TiO_2 and synthesis of the hardest known oxide. Journal of Physics-Condensed Mattter, 14, 10995–10999.

Akahama, Y., and Kawamura, H. (2006) Pressure calibration of diamond anvil Raman gauge to 310 GPa. Journal of Applied Physics, 100, 043516.

Al-Khatatbeh, Y., Lee, K. K. M., and Kiefer, B. (2009) High-pressure behavior of TiO_2 as determined by experiment and theory. Physical Review B, 79, 134114.

Angel, R. J., Bujak, M., Zhao, J., Gatta, G. D., and Jacobsen, S. D. (2007) Effective hydrostatic limits of pressure media for high-pressure crystallographic studies. Journal of Applied Crystallography, 40, 26–32.

Carr, J., and Hampson, N. (1972) Lead dioxide electrode. Chemical Reviews, 72, 679-703.

Chen, S., and Shen, P. (2002) Laser ablation condensation of α-PbO_2-type TiO_2. Physical Review Letters, 89, 096106.

Dekura, H., Tsuchiya, T., Kuwayama, Y., and Tsuchiya, J. (2011) Theoretical and Experimental Evidence for a New Post-Cotunnite Phase of Titanium Dioxide with Significant Optical Absorption. Physical Review Letters, 107, 045701.

Desgreniers, S. and Lagarec, K. (1999) High-density ZrO_2 and HfO_2: Crystalline structures and equations of state. Physical Review B, 59(13), 8467-8472.

Dewhurst, J., and Lowther, J. (2001) Highly coordinated metal dioxides in the cotunnite structure. Physical Review B, 64, 014104.

Dorfman, S. M., Jiang, F., Mao, Z., Kubo, A., Meng, Y., Prakapenka, V. B., and Duffy, T. S. (2010) Phase transitions and equations of state of alkaline earth fluorides CaF_2, SrF_2, and BaF_2 to Mbar pressures. Physical Review B, 81, 174121.

Dubrovinskaia, N., Dubrovinsky, L., Ahuja, R., Prokopenko, V., Dmitriev, V., Weber, H., Osorio-Guillen, J., and Johansson, B. (2001) Experimental and theoretical identification of a new high-pressure TiO_2 polymorph. Physical Review Letters, 87, 275501.

Dubrovinsky, L., Saxena, S., Lazor, P., Ahuja, R., Eriksson, O., Wills, J., and Johansson, B. (1997) Experimental and theoretical identification of a new high-pressure phase of silica. Nature, 388, 362–365.

Dubrovinsky, L., Dubrovinskaia, N., Saxena, S., Tutti, F., Rekhi, S., Le Bihan, T., Shen, G., and Hu, J. (2001a) Pressure-induced transformations of cristobalite. Chemical Physics Letters, 333, 264–270.

Dubrovinsky, L. S., Dubrovinskaia, N. A., Swamy, V., Muscat, J., Harrison, N. M., Ahuja, R., Holm, B., and Johansson, B. (2001b) The hardest known oxide. Nature, 410, 653-654.

El Goresy, A., Chen, M., Gillet, P., Dubrovinsky, L., Graup, G., and Ahuja, R. (2001) A natural shock-induced dense polymorph of rutile with α-PbO_2 structure in the suevite from the Ries crater in Germany. Earth and Planetary Science Letters, 192, 485–495.

Griffiths, G. I. G., Needs, R. J., and Pickard, C. J. (2009) Post-cotunnite phase of TeO_2 obtained from first-principles density-functional theory methods with random-structure searching. Physical Review B, 80, 184115.

Fiquet, G., Andrault, D., Itie, J.P., Gillet, P., and Richet, P. (1996) X-ray diffraction of ferropericlase in a laser-heated diamond-anvil cell. Physics of the Earth and Planetary Interiors, 95, 1-17.

Grocholski, B., Shim, S. H., and Prakapenka, V. B. (2010) Stability of the $MgSiO_2$ analog $NaMgF_3$ and its implication for mantle structure in super-Earths. Geophysical Research Letters, 37, L14204.

Grocholski, B., Shim, S., and Prakapenka, V. B. (2013) Stability, metastability, and elastic properties of a dense silica polymorph, seifertite. Journal of Geophysical Research Solid Earth, in review.

Haines, J., Leger, J., and Schulte, O. (1996) The high-pressure phase transition sequence from the rutile-type through to the cotunnite-type structure in PbO_2. Journal of Physics-Condensed Matter, 8, 1631–1646.

Haines, J., and Leger, J. (1997) X-ray diffraction study of the phase transitions and structural evolution of tin dioxide at high pressure: Relationships between structure types and implications for other rutile-type dioxides. Physical Review B, 55, 11144–11154.

Haines, J., Leger, J., and Schulte, O. (1998) High-pressure isosymmetric phase transition in orthorhombic lead fluoride. Physical Review B, 57, 7551–7555.

Heinz, D. L., and Jeanloz, R. (1987) Measurement of the melting curve of Mg0.9Fe0.1SiO3 at lower mantle conditions and its geophysical implications. Journal of Geophysical Research, 92(B11), 11437–11444.

Heinz, D. L. (1990) Thermal pressure in the laser-heated diamond anvil cell. Geophysical Research Letters, 17, 1161–1164.

Larson, A., and Von Dreele, R. (2000) General structure analysis system. Los Alamos National Laboratory Report LAUR, pp. 86–748.

Leger, J., Haines, J., Atouf, A., Schulte, O., and Hull, S. (1995) High-Pressure X-ray diffraction and neutron diffraction studies of BaF_2 - An example of a coordination number of 11 in AX_2 compounds. Physical Review B, 52, 13247–13256.

Leger, J., Haines, J., and Danneels, C. (1998) Phase transition sequence induced by high-pressure in $CaCl_2$. Journal of the Physics and Chemistry of Solids. 59(8), 1199-1204.

Lowther, J., Dewhurst, J., Leger, J., and Haines, J. (1999) Relative stability of ZrO_2 and HfO_2 structural phases. Physical Review B, 60, 14485–14488.

Mao, H.-K., Xu, J., and Bell, P. M. (1986) Calibration of the ruby pressure gauge to 800 kbar under quasihydrostatic conditions. Journal of Geophysical Research, 91, 4673–4676.

Ohtaka, O., Andrault, D., Bouvier, P., Schultz, E., and Mezouar, M. (2005) Phase relations and equation of state of ZrO_2 to 100 GPa. Journal of Applied Physics, 38, 727–733.

Ohtaka, O., Fukui, H., Kunisada, T., Fujisawa, T., Funakoshi, K., Utsumi, W., Irifune, T., Kuroda, K., and Kikegawa, T. (2001a) Phase relations and volume changes of hafnia under high pressure and high temperature. Journal of the American Ceramics Society, 84, 1369–1373.

Ohtaka, O., Fukui, H., Kunisada, T., Fujisawa, T., Funakoski, K., Utsumi, W., Irifune, T., Kuroda, K., and Kikegawa, T. (2001b) Phase relations and equations of state of ZrO_2 under high temperature and high pressure. Physical Review B, 63, 174108.

Prakapenka, V., Dubrovinsky, L., Shen, G., Rivers, M., Sutton, S., Dmitriev, V., Weber, H., and Le Bihan, T. (2003) α-PbO_2-type high-pressure polymorph of GeO_2. Physical Review B, 67, 132101.

Prakapenka, V. B., Kubo, A., Kuznetsov, A., Laskin, A., Shkurikhin, O., Dera, P., Rivers, M. L., and Sutton, S. R. (2008) Advanced flat top laser heating system for high pressure research at GSECARS: application to the melting behavior of germanium. High Pressure Research, 28, 225–235, International Workshop on Synchrotron High-Pressure Mineral Physics and Materials Science, Chicago, IL, DEC 06-07, 2007.

Ross, M., Mao, H., Bell, P., and Xu, J. (1986) The equation of state of dense argon - A comparison of shock and static studies. Journal of Chemical Physics, 85, 1028–1033.

Sharp, T., El Goresy, A., Wopenka, B., and Chen, M. (1999) A post-stishovite SiO_2 polymorph in the meteorite Shergotty: Implications for impact events. Science, 284, 1511–1513.

Shieh, S., Duffy, T., and Shen, G. (2005) X-ray diffraction study of phase stability in SiO_2 at deep mantle conditions. Earth and Planetary Science Letters, 235, 273–282.

Shieh, S., Kubo, A., Duffy, T., Prakapenka, V., and Shen, G. (2006) High-pressure phases in SnO_2 to 117 GPa. Physical Review B, 73, 014105.

Taggart, J., Foord, E., Rosenzweig, A., and Hanson, T. (1988) Scrutinyite, natural occurrences of α-PbO_2 from Bingham, New Mexico, USA, and Mapimi, Mexico. Canadian Mineralogist, 26, 905–910.

Teter, D. (1998) Computational alchemy: The search for new superhard materials. Materials Research Society Bulletin, 23, 22–27.

Tsuchiya, T., and Tsuchiya, J. (2011) Prediction of a hexagonal SiO_2 phase affecting stabilities of $MgSiO_3$ and $CaSiO_3$ at multimegabar pressures. Proceedings of the National Academy of Sciences USA, 108, 1252–1255.

Umemoto, K., Wentzcovitch, R., and Allen, P. (2006) Dissociation of $MgSiO_3$ in the cores of gas giants and terrestrial exoplanets. Science, 311, 983–986.

Xia, X., Weidner, D. J., and Zhao, H. (1998) Equation of state of brucite: Single-crystal Brillouin spectroscopy study and polycrystalline pressure-volume-temperature measurement. American Mineralogist, 83, 68–74.

Figure 1: Stability diagram for high-pressure phases of PbO_2. Blue denotes where the cotunnite-type (*Pnam*) phase is found, red for OI-type (*Pbca*), green for trace baddeleyite-type ($P2_1/c$), pink for pyrite-type (*Pa*-3), and black for the α-structure (*Pbcn*). Circles denote the stable phase during and after heating, triangles denote stable phases during cold compression or post-annealing decompression, and crosses denote where there is evidence of melting. The pressure values are from the room temperature measurements and so we have used asymmetric error bars to account for the likely effect of thermal pressure at high temperature. Experimental values for cold compression and decompression from Haines et al. (1996) are presented at the bottom. The cotunnite transition is hindered at low pressure, with the OI phase remaining metastable well into the stability field of the cotunnite-type phase. Heating (this study) or shear stress (Haines et al, 1996) may produce the high pressure phase, although with the latter method a large modal fraction remains in the OI structure.

Figure 2: Full width at half maximum (FWHM) of the 100% line for laser annealed samples (red circles), unheated samples (blue squares), decompression measurements (green triangles), and measurements collected using silicone grease (open squares), (Haines et al., 1996). Error from FWHM fits are much smaller than the scatter between diffraction patterns collected at similar pressure. Lines are best fit from linear regression. The FWHM in our unheated samples is much lower than the silicone grease results due to our use of argon pressure medium, with annealing of the samples sharpening diffraction peaks by an additional factor of 2–3. The arrow shows the result of decompression from 75.1 GPa on the FWHM, which results in peak broadening of a similar magnitude to cold compression over a similar pressure range.

Figure 3: Examples of measured X-ray diffraction patterns with background subtraction (black lines) along with fits (red lines) and residuals (blue lines) obtained from Rietveld refinements. The omitted intensity between 14.5° and 15.5° is due to the angled part of the cBN seat and not included in the structural refinement. The vertical bars represent peak positions obtained from structural refinements. (A) Example of diffraction pattern from the OI structure obtained on initial compression to 34.5 GPa of the starting material. A small amount of baddeleyite-structured material helps account for the shoulders around the most intense line. (B) Cotunnite structure obtained at 39 GPa post-heating at ~1500 K. The changes in diffraction patterns and peak sharpening from (A) to (B) are typical after only a few minutes of laser heating (see Fig. 4 as well). (C) Cotunnite structure compressed to 105 GPa at room temperature without laser heating of the sample. (D) Post-heating diffraction of (C), resulting in significant sharpening of the cotunnite-type phase reflections (E) Pyrite-type structure with minor amounts of baddeleyite and OI type phases formed on decompression of the cotunnite-type phase from 24 GPa to 10.5 GPa. (F) Unheated PbO_2 in the α structure after room temperature decompression from (E) at 10.5 GPa.

Figure 4: (A) Example of unheated diffraction pattern collected at 75 GPa. Diffraction lines are broad and distorted from non-hydrostatic stresses. (B) Example of unrolled diffraction pattern collected post-heating at 75 GPa. The quality in the 2-dimensional and integrated patterns is typical for PbO_2 samples after a few minutes of laser heating. The angular range is greater than for the unheated pattern because we moved the detector closer to the sample. (C) Rietveld structural refinement (red) of the diffraction pattern of PbO_2 (black) at 75.1 GPa and residual (blue) after background fit (dashed line). A total of 89 different reflections (red vertical bars) were used in the fitting, omitting the two reflections that occur in the angular range where the x-rays transit through the angled part of the cBN seat.

Figure 5: Crystal structure model of the cotunnite-type phase in PbO_2 looking close to straight down the *c*-axis. Red spheres are oxygen atoms and black spheres are lead atoms. The nine-fold coordinated structure consists of three sets of bonds with a two-fold multiplicity labeled 2, 5, and 6. Bonds 1, 3, and 4 have a multiplicity of one. The oxygen network is a distorted hcp lattice that forms kinked chains of coordinating polyhedra.

Figure 6: Pb–O bond lengths from structural refinements of cotunnite structure and Pb-Pb-Pb angles. Most Pb-O bond distances decrease rapidly with pressure, before flattening out at even higher pressure. The trend is to have more uniform bond distances, although there is still appreciable scatter from the refinements. The Pb-Pb-Pb angles become slightly less regular with pressure.

Figure 7: Lattice parameters from our data set (filled) and from Haines et al. (1996) (open). Dashed lines are fits to the unit cell parameters that are back-extrapolated to room pressure for the cotunnite-type structure using the method in Xia et al. (1998). This yields a_0=5.663(4), b_0=6.670(4), c_0=3.563(3). The cotunnite-type structure has close to isotropic compression. The compressibility is in contrast to the OI structure, where the *b* axis is much stiffer than the *a* or *c* axes (see Tab. 3**).** The *a*/*c* ratio is shown, which increases and levels off like ZrO_2 (Ohtaka et al., 2001) and SnO_2 (Shieh et al., 2005). The a/c ratio for flouride compounds such as CaF_2 (open blue cirlces) has a decrease when approaching the post-cotunnite transition (Dorfman et al., 2010). Although the decrease in our ratio above 120 GPa is slight, it may be an early indication of a phase transition at slightly higher pressure.

Figure 8: Lattice parameters for lower pressure phases. Our data is consistent with the previous results (Haines et al, 1996). However, we find our lattice parameters of the OI structure systematically lower above 29 GPa. The discrepancy is likely due to severe peak overlaps from deviatoric stresses in the previous results.

Figure 9: Measured unit cell volumes for OI ($Z = 8$) and cotunnite ($Z = 4$) phases. The error is smaller than the size of the data points (Tab. 2). The volume change at the transition (24 GPa) is 11%, consistent with other analogs such as ZrO_2 (Ohtaka et al., 2001). Dashed lines are fits to the second-order Birch Murnaghan EOS. This yields a $K_0 = 219(1)$ GPa with $V_0 = 134.4(3)$ Å^3 for the cotunnite structure and $K_0 = 122(7)$ GPa with $V_0 = 313.8(1.9)$ for the OI structure.

Table 1: Atomic coordinates obtained from the Rietveld refinements. The z-coordinate is 0.25, 0.25, and 0.75 for Pb, O1, and O2, respectively.

P (GPa)	x_{Pb}	y_{Pb}	x_{O1}	y_{O1}	x_{O2}	y_{O2}
23.5(5)	0.260(1)	0.100(2)	0.317(3)	0.409(3)	0.087(4)	0.346(2)
29.0(6)	0.254(1)	0.100(2)	0.335(2)	0.415(2)	0.071(3)	0.365(2)
39.0(8)	0.258(1)	0.103(1)	0.338(4)	0.440(3)	0.061(5)	0.344(3)
62.7(1.2)	0.257(1)	0.108(1)	0.344(3)	0.416(2)	0.020(4)	0.321(2)
75.1(1.5)	0.256(1)	0.109(1)	0.361(2)	0.413(1)	0.039(2)	0.322(1)
93(3)	0.255(1)	0.111(1)	0.332(3)	0.416(2)	0.073(4)	0.315(2)
105(3)	0.259(1)	0.113(1)	0.344(2)	0.407(2)	0.079(3)	0.296(3)
120(2)	0.251(1)	0.109(1)	0.360(3)	0.428(4)	0.079(5)	0.339(4)
140(2)	0.255(1)	0.110(1)	0.347(2)	0.440(2)	0.110(5)	0.317(4)

Table 2: Pressures and lattice parameters for cotunnite-type lead dioxide.

P (GPa)	*a* (Å)	*b* (Å)	*c* (Å)	vol (Å^3)	*a*/*c*
23.5(5)	5.493(2)	6.520(2)	3.453(2)	123.7(1)	1.591(1)
29.0(6)	5.464(3)	6.468(4)	3.415(2)	120.7(2)	1.600(1)
34.5(6)	5.446(3)	6.426(3)	3.383(3)	118.4(2)	1.610(2)
39.0(8)	5.426(3)	6.389(2)	3.362(2)	116.6(1)	1.614(1)
62.7(1.2)	5.343(4)	6.290(2)	3.295(4)	110.7(2)	1.622(2)
75.1(1.5)	5.298(3)	6.239(3)	3.269(3)	108.1(2)	1.620(2)
93(3)	5.246(3)	6.194(3)	3.228(3)	104.9(2)	1.625(2)
105(3)	5.215(3)	6.167(4)	3.211(4)	103.3(2)	1.624(2)
120(2)	5.128(4)	6.108(3)	3.183(3)	99.7(2)	1.611(2)
129(2)	5.107(3)	6.084(3)	3.163(3)	98.3(1)	1.615(2)
135(2)	5.085(4)	6.061(4)	3.155(4)	97.2(2)	1.612(2)
140(2)	5.083(2)	6.046(2)	3.152(4)	96.9(1)	1.613(2)

Table 3: Unit-cell parameters and elastic parameters for OI and cotunnite-type phase for PbO_2, with K'_0 fixed at 4. Linear bulk moduli of the unit-cell axes were computed with the method of Xia1998.

	a_0 (Å)	K_{0a} (GPa)	b_0 (Å)	K_{0b} (GPa)	c_0 (Å)	K_{0c} (GPa)	V_0 (Å^3)	K_0 (GPa)
				OI				
This study	10.749(40)	82(7)	5.380(10)	286(33)	5.477(30)	77(6)	313.8(1.9)	122(7)
Haines (1996)	—	—	—	—	—	—	304.0	180(7)
				Cotunnite-type				
This study	5.663(4)	227(1)	6.670(4)	259(4)	3.563(3)	174(1)	134.4(3)	219(3)
Haines (1996)	—	—	—	—	—	—	135.38	221(21)

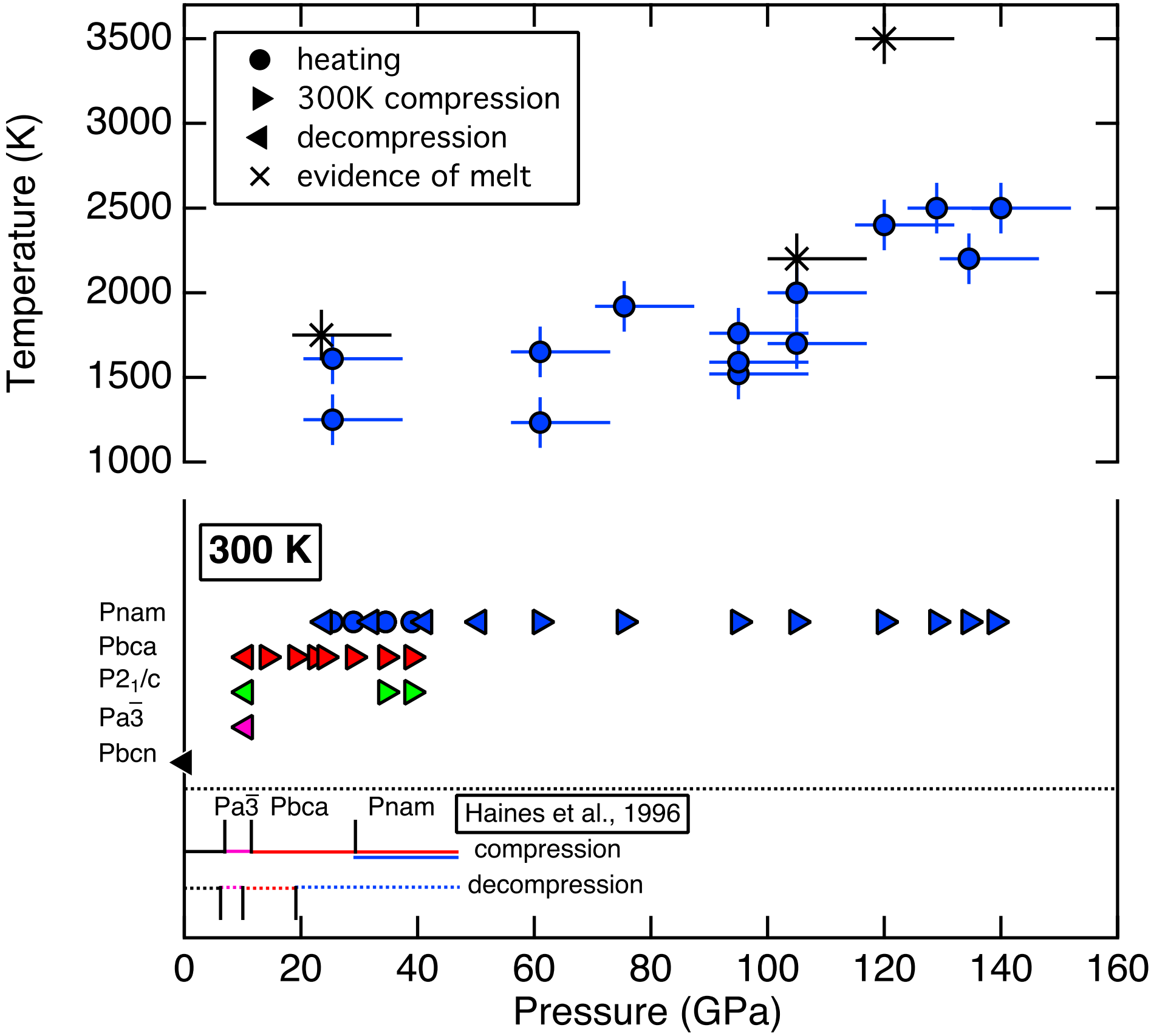
heating
300K compression
decompression
evidence of melt
Temperature (K)
3500
3000
2500
2000
1500
1000
300 K
Pnam
Pbca
P2$_1$/c
Pa$\bar{3}$
Pbcn
Pa$\bar{3}$ Pbca Pnam
Haines et al., 1996
compression
decompression
0
20
40
60
80
100
120
140
160
Pressure (GPa)

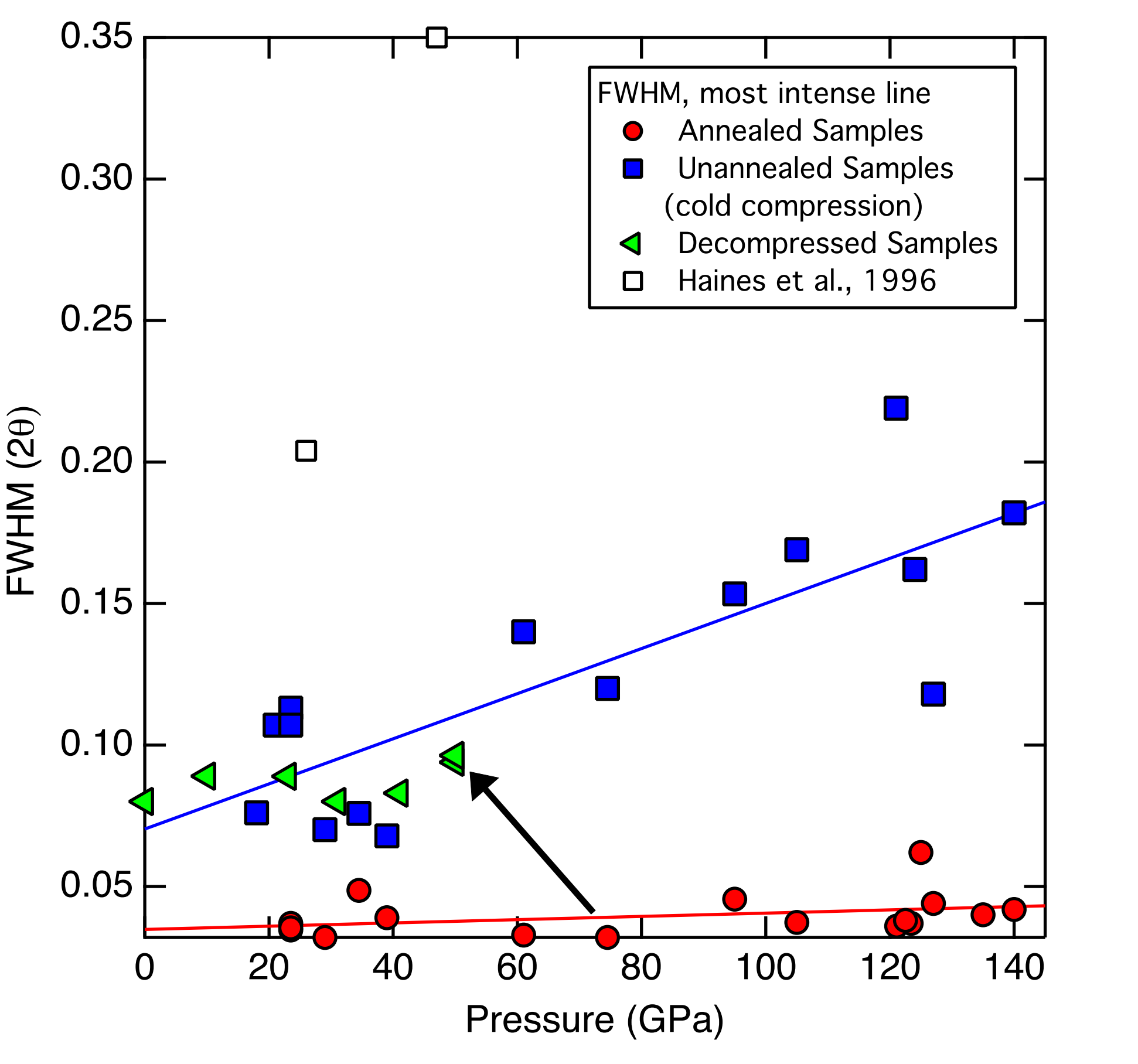
FWHM, most intense line
Annealed Samples
Unannealed Samples
(cold compression)
Decompressed Samples
Haines et al., 1996
FWHM (2θ)
Pressure (GPa)
0.35
0.30
0.25
0.20
0.15
0.10
0.05
0
20
40
60
80
100
120
140

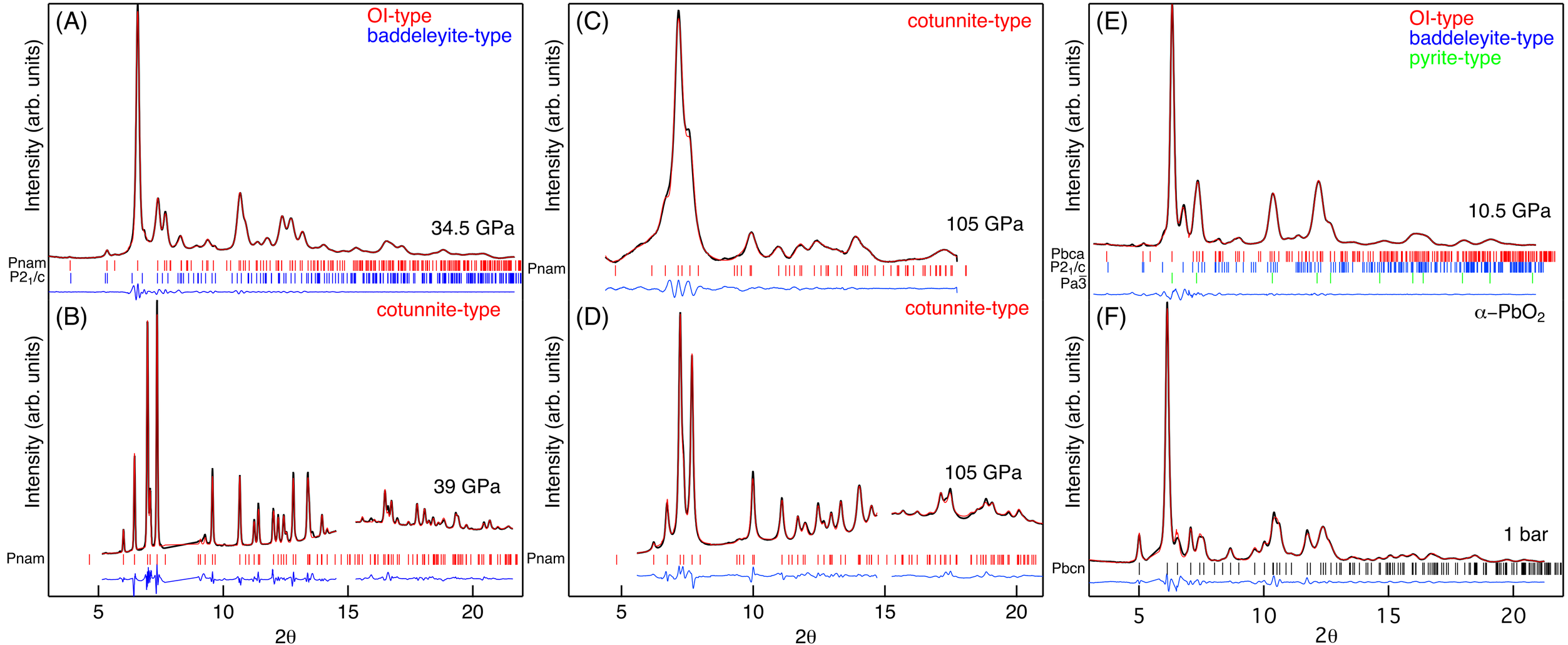
(A)
OI-type
baddeleyite-type
34.5 GPa
Pnam
P2$_1$/c
(B)
cotunnite-type
39 GPa
Pnam
(C)
cotunnite-type
105 GPa
Pnam
(D)
cotunnite-type
105 GPa
Pnam
(E)
OI-type
baddeleyite-type
pyrite-type
10.5 GPa
Pbca
P2$_1$/c
Pa3̄
(F)
α–PbO$_2$
1 bar
Pbcn
Intensity (arb. units)
2θ
5
10
15
20

(A)

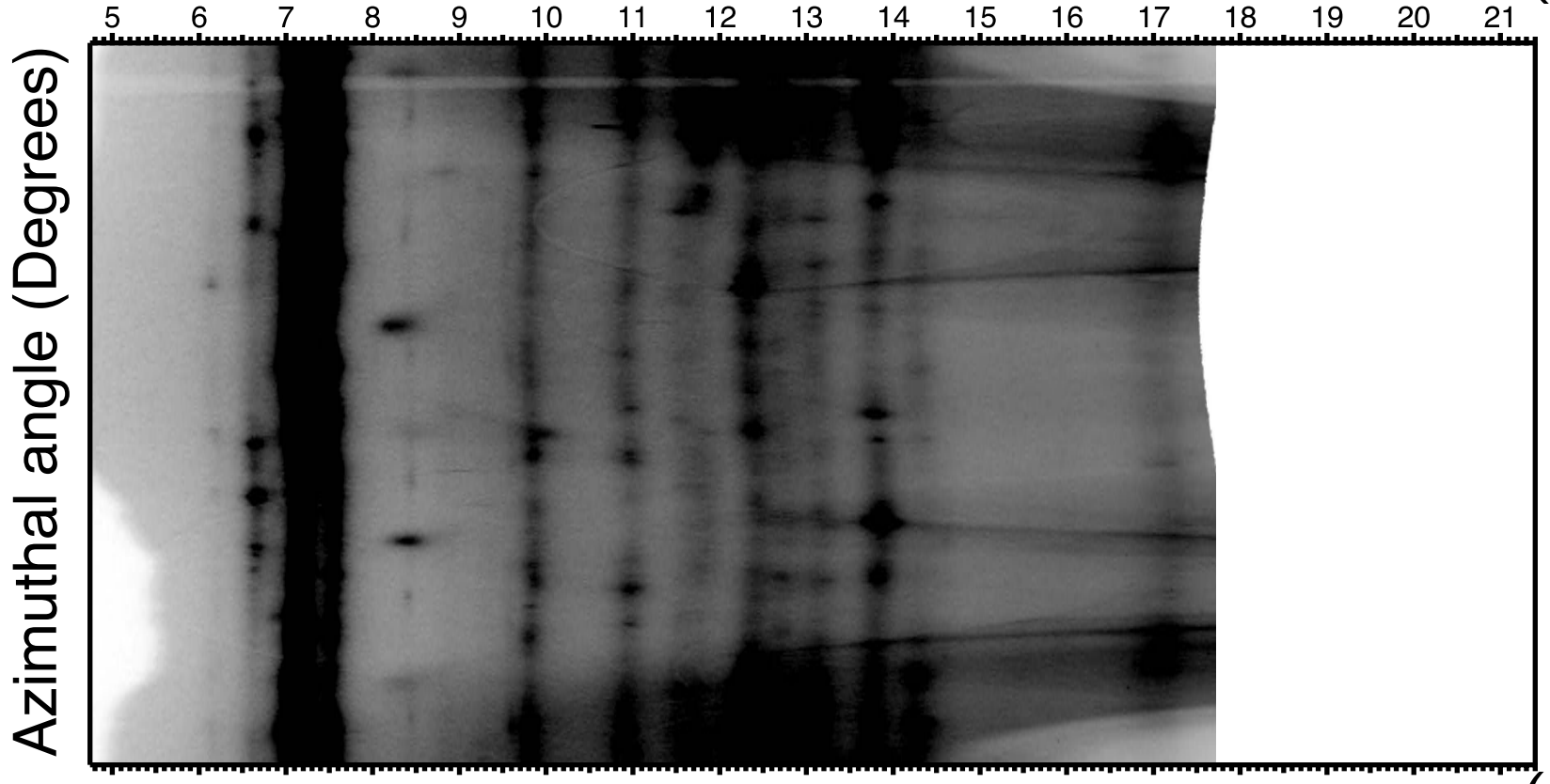
5 6 7 8 9 10 11 12 13 14 15 16 17 18 19 20 21
Azimuthal angle (Degrees)

(B)

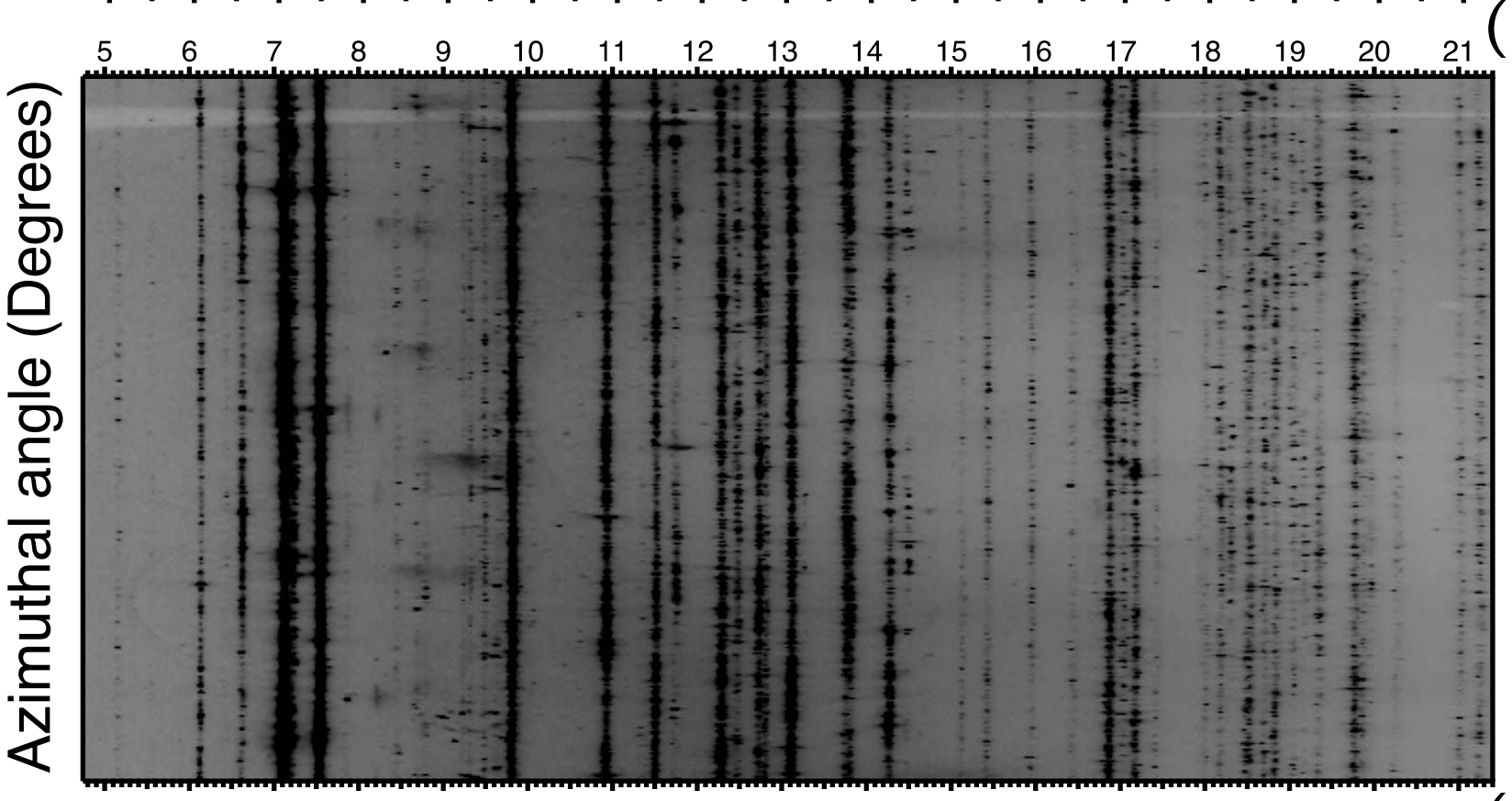
5 6 7 8 9 10 11 12 13 14 15 16 17 18 19 20 21
Azimuthal angle (Degrees)

(C)

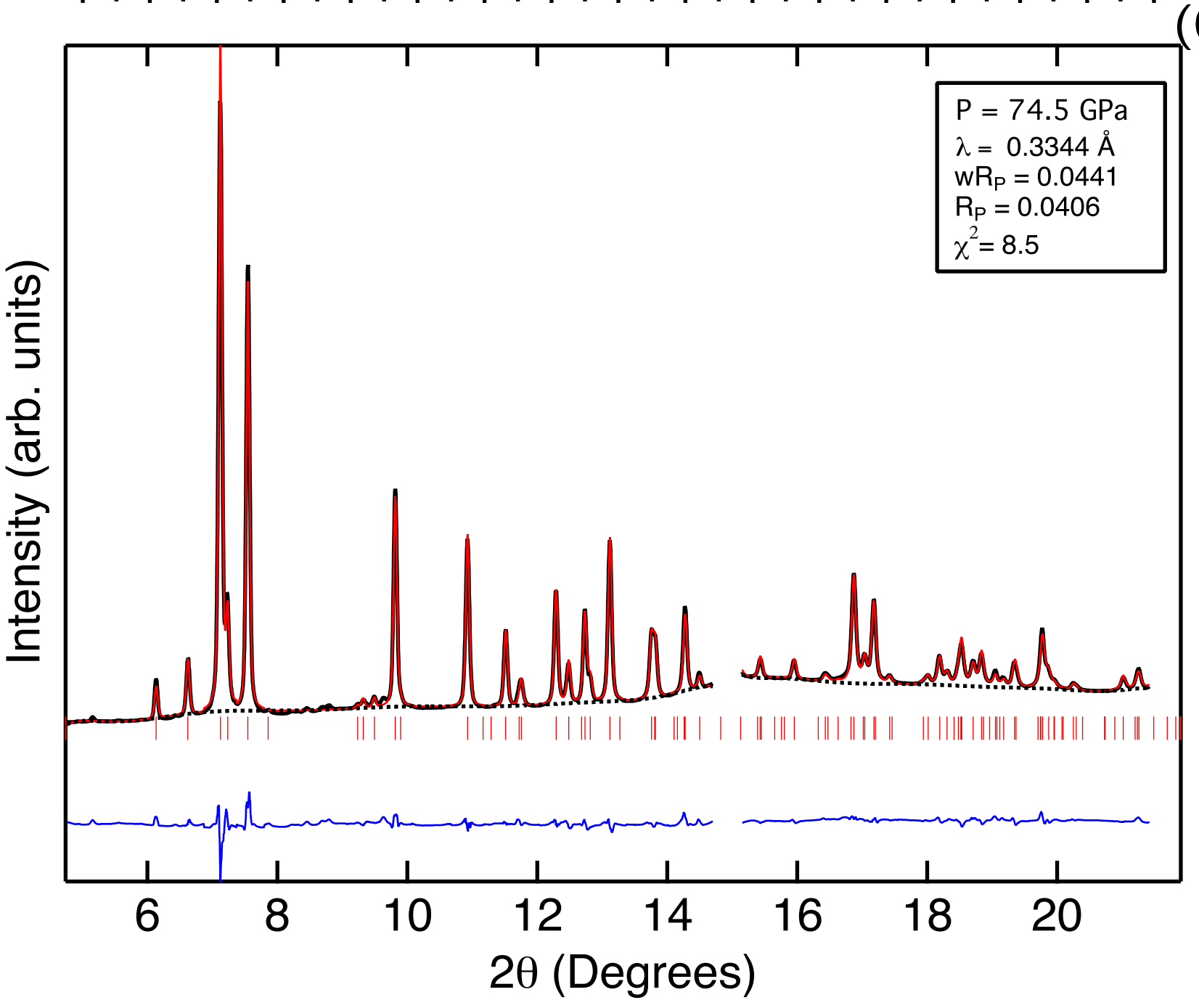
P = 74.5 GPa
λ = 0.3344 Å
wR$_P$ = 0.0441
R$_P$ = 0.0406
χ^2 = 8.5
Intensity (arb. units)
6 8 10 12 14 16 18 20
2θ (Degrees)

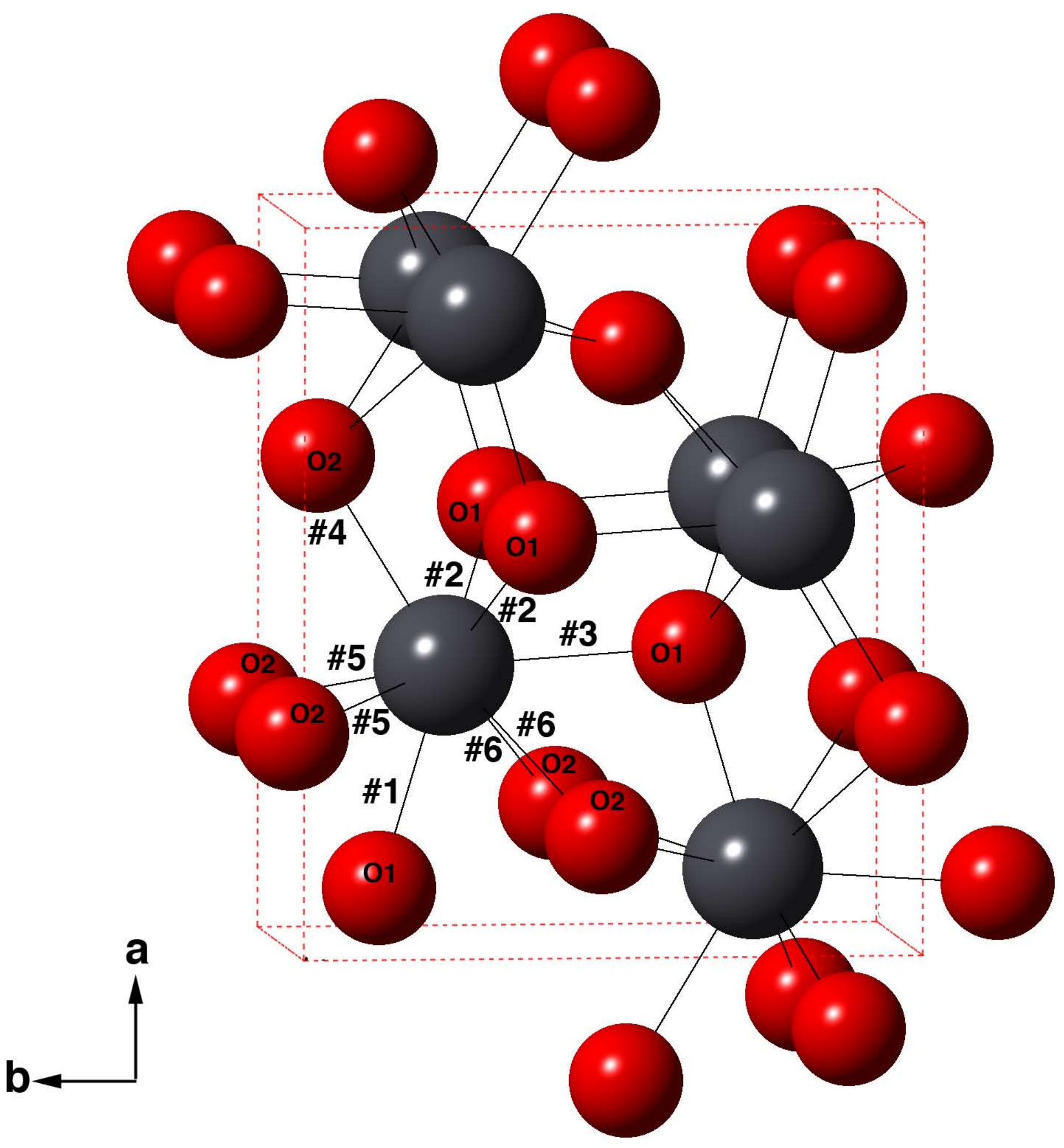
O2
O1
#4
O1
#2
#2
#3
O1
#5
O2
O2
#5
#6
#6
O2
O2
#1
O1
a
b

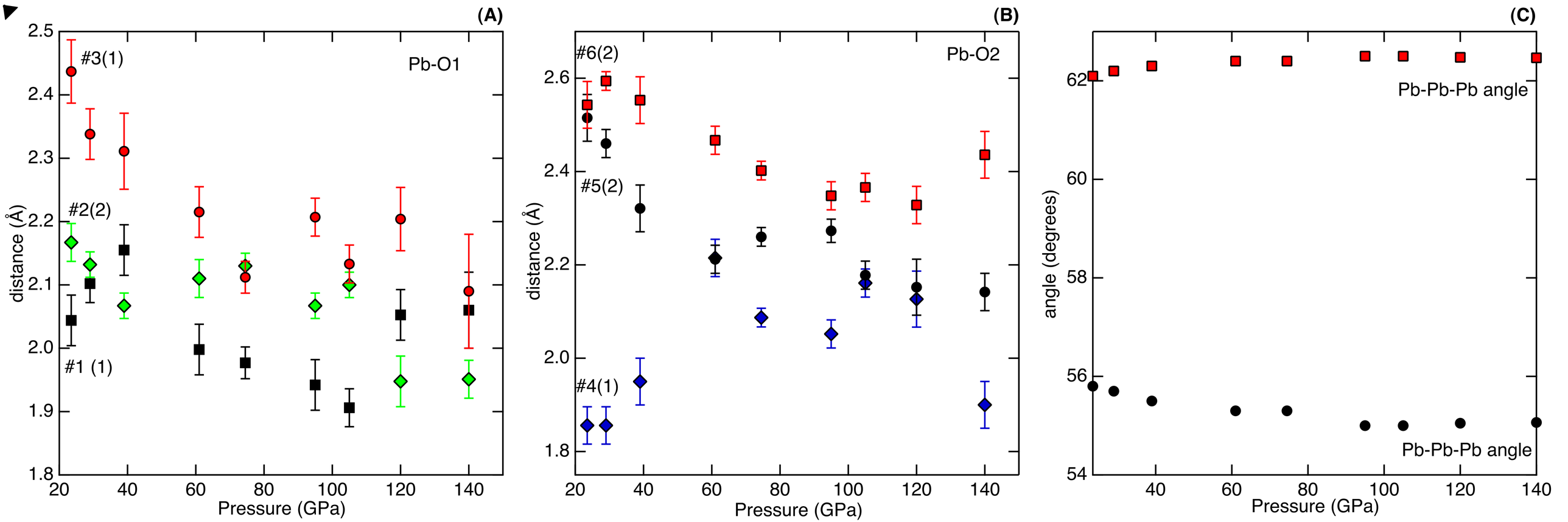
(A)
Pb-O1
#3(1)
#2(2)
#1 (1)
distance (Å)
Pressure (GPa)
(B)
Pb-O2
#6(2)
#5(2)
#4(1)
distance (Å)
Pressure (GPa)
(C)
Pb-Pb-Pb angle
Pb-Pb-Pb angle
angle (degrees)
Pressure (GPa)

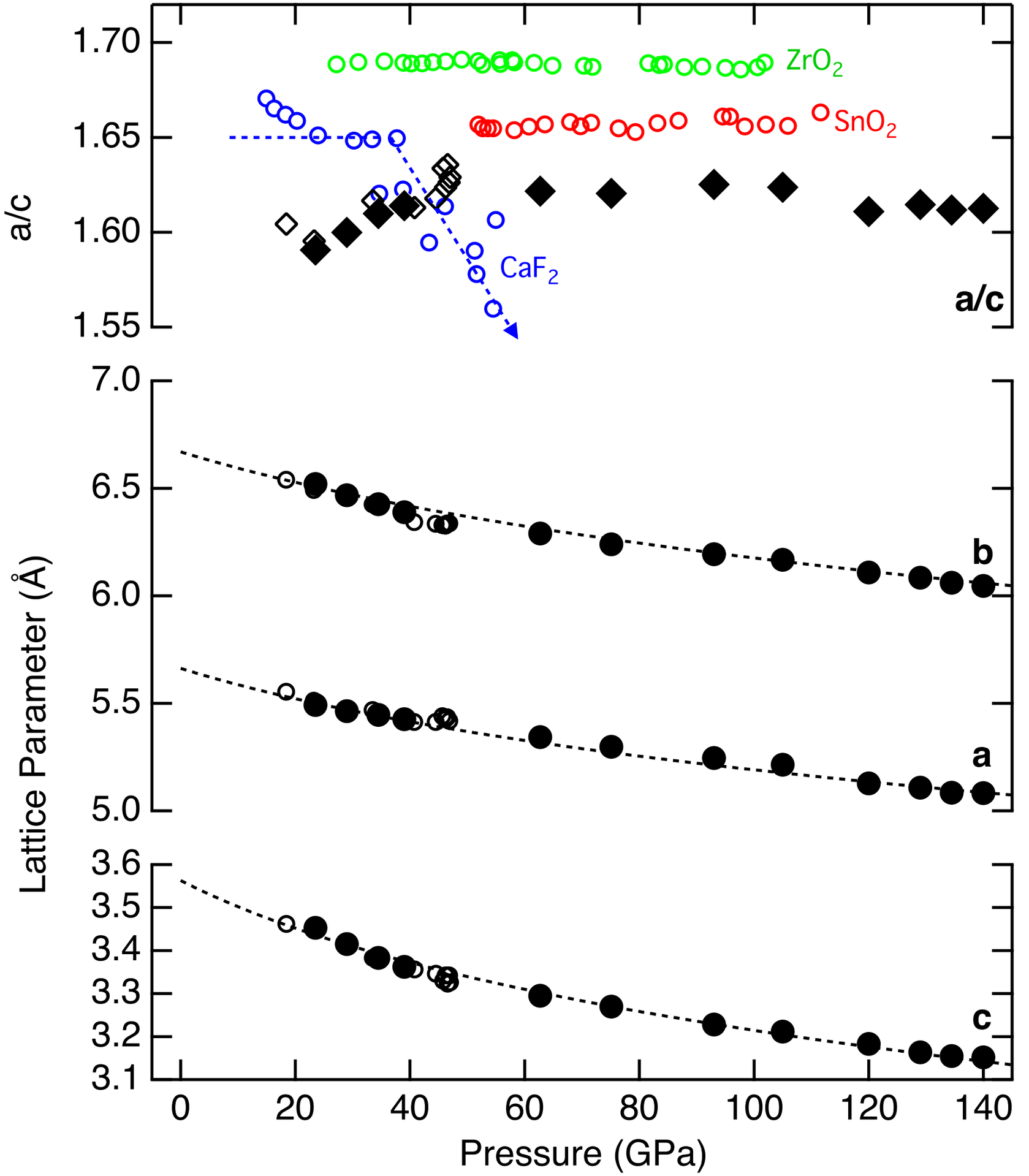
a/c
1.70
1.65
1.60
1.55
ZrO2
SnO2
CaF2
a/c
Lattice Parameter (Å)
7.0
6.5
6.0
5.5
5.0
3.6
3.5
3.4
3.3
3.2
3.1
b
a
c
0
20
40
60
80
100
120
140
Pressure (GPa)

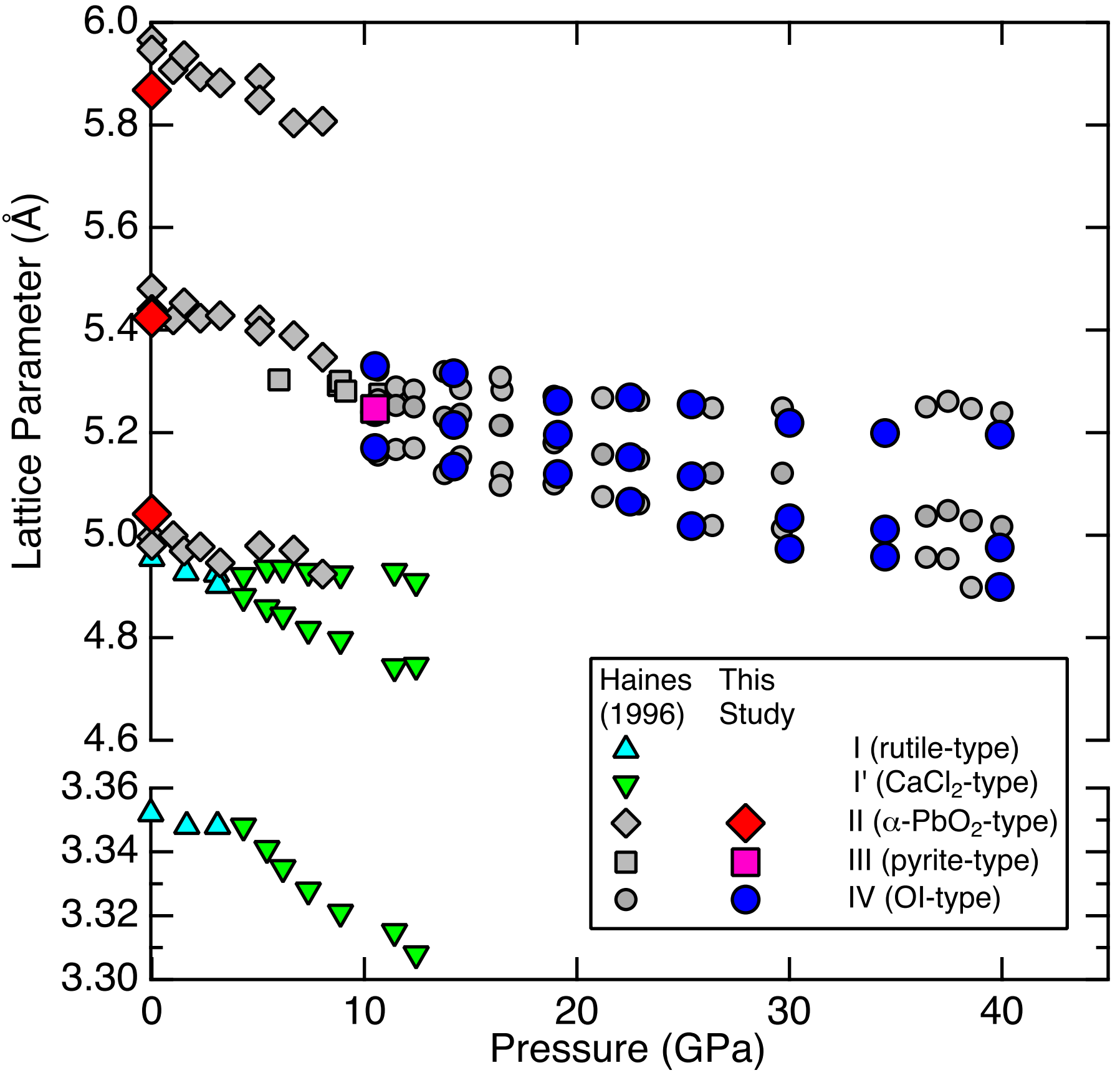
Lattice Parameter (Å)
Pressure (GPa)
6.0
5.8
5.6
5.4
5.2
5.0
4.8
4.6
3.36
3.34
3.32
3.30
0
10
20
30
40
Haines (1996)
This Study
I (rutile-type)
I' (CaCl2-type)
II (α-PbO2-type)
III (pyrite-type)
IV (OI-type)

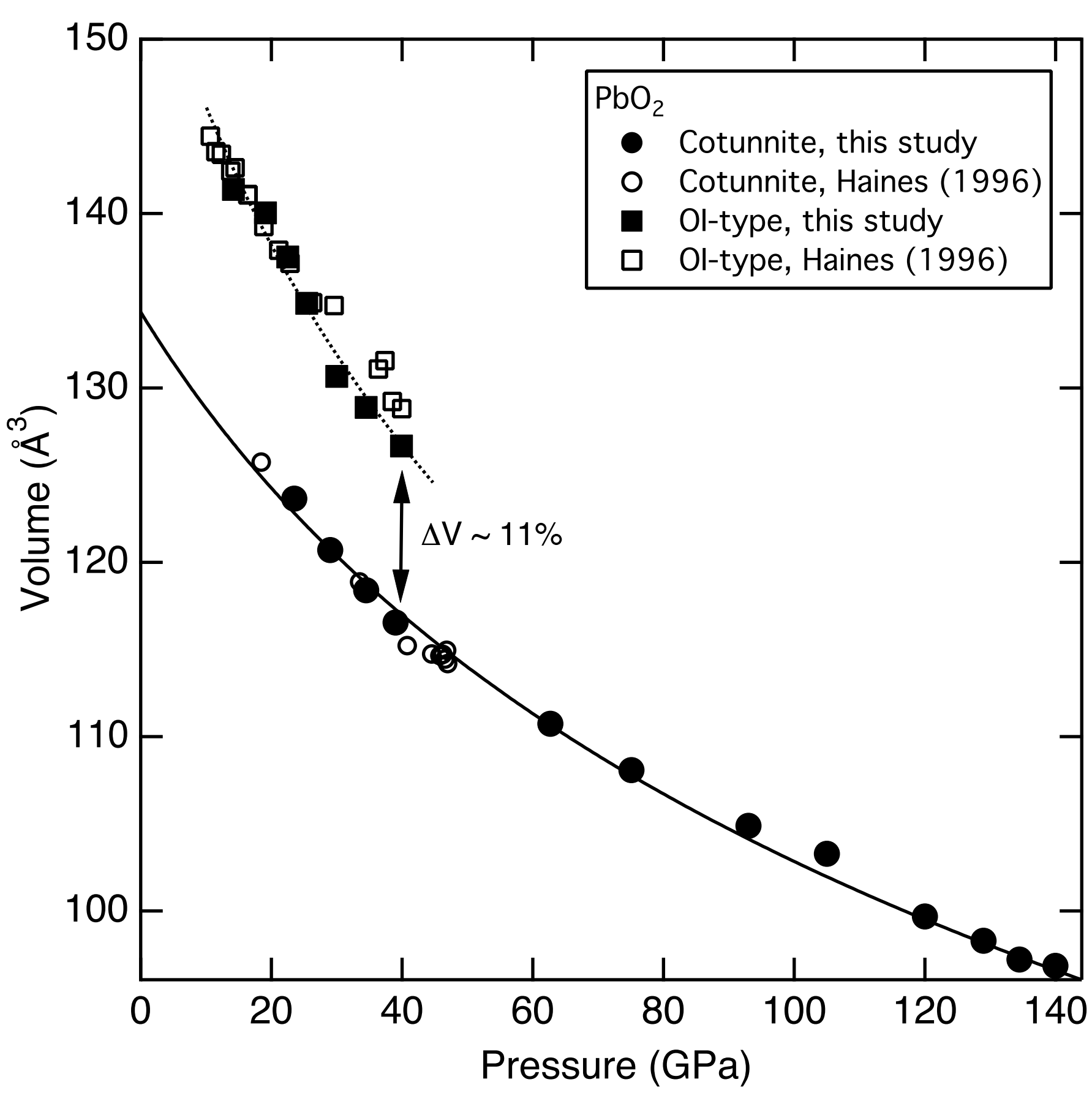
PbO2
Cotunnite, this study
Cotunnite, Haines (1996)
OI-type, this study
OI-type, Haines (1996)
ΔV ~ 11%
Volume (Å3)
Pressure (GPa)
150
140
130
120
110
100
0
20
40
60
80
100
120
140